VISIT…

2

Determination of mechanical properties

2.1 Introduction

Mechanical testing of engineering materials may be carried out for a number of reasons: The tests may simulate the service conditions of a material, so that the test results may be used to predict its *service performance*. Mechanical testing may also be conducted in order to provide engineering *design data*, as well as *acceptability*, the main purpose of which is to check whether the material meets the specification.

In the USA, the American Society for Testing Materials (ASTM) publish standard specifications and methods of testing which are updated every three years. In the UK, the British Standards Institution (BSI) publish an annual catalogue of all BSI Standards, and agreed European Standards (EN series). All of these organizations issue publications relating to the selection of test-pieces and the conducting of mechanical tests. We will consider a number of these tests in turn.

2.2 The tensile test

The tensile test is widely used for measuring the stiffness, strength and ductility of a material. The testing machine subjects the test-piece to an axial *elongation* and the resultant *load* on the specimen is measured. Depending on the nature of the product being tested, the specimen may be round or rectangular in cross-section, with the region between the grips usually being of reduced cross–section. The *gauge length* is marked in this region.

We will consider the response of a ductile metal as an illustration. The load–elongation data are normally converted to stress and strain:

Stress = Load/Cross-sectional area
Strain = Extension of gauge length/Original gauge length

Figure 2.1 illustrates the behaviour at small strains. The linear part of the curve may correspond to easily measured elongations in some polymeric

© Woodhead Publishing Limited, 2006

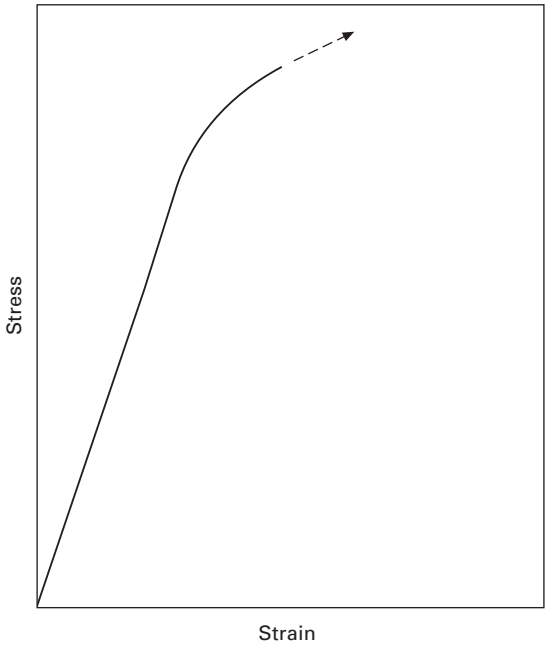

2.1 Tensile test at small strains.

materials, but in metals the displacements are very small and usually require the use of an *extensometer* or *resistance strain-gauge* to measure them with sufficient accuracy.

This part of the curve, described by Hooke's Law, represents *elastic* behaviour. Its slope corresponds to Young's modulus (E), which is given by the ratio of stress to strain. We have seen in Fig. 0.1, which plots Young's modulus vs. density for engineering materials, that the value of Young's modulus can vary by over three orders of magnitude for different materials with elastomers having values of the order 0.1 GPa and metals and ceramics having values of hundreds of gigapascals.

It is clearly important for design engineers to know the stress at which elastic behaviour ceases. The *limit of proportionality* is the highest stress that can be applied with Hooke's Law being obeyed and the *elastic limit* is the maximum stress that can be applied without causing permanent extension to the specimen. Neither of these stresses will be found in reference books of properties of materials, however, since their experimental measurement is fraught with difficulty. The more sensitive the strain gauge employed in the experiment, the lower the limit of proportionality and the elastic limit will appear to be. Thus, as one changes from mechanical measurement of the strain with, say, a micrometer, to an optical lever device then to an electrical resistance strain gauge and, finally, to optical interferometry one would detect

© Woodhead Publishing Limited, 2006

departure from elastic behaviour (as defined above) at progressively lower stresses, due to the presence of *microstrains*.

Departure from elasticity is therefore defined in an empirical way by means of a *proof stress*, the value of which is independent of the accuracy of the strain-measuring device. Having constructed a stress–strain curve as in Fig. 2.1, an arbitrary small strain is chosen, say 0.1 or 0.2%, and a line parallel to Young's modulus is constructed at this strain. The point of intersection of this line with the stress–strain curve defines the 0.1 or 0.2% *proof stress* and values of this stress for different materials are available in books of reference, since they provide an empirical measure of the limit of elastic behaviour. In the USA this stress is known as the *offset yield strength.*

The Bauschinger Effect

If a metallic specimen is deformed plastically in tension up to a tensile stress of $+\sigma_t$ (Fig. 2.2) and is then subjected to a *compressive* strain (as indicated by the arrows in Fig. 2.2), it will first contract elastically and then, instead of yielding plastically in compression at a stress of $-\sigma_t$ as might have been expected, it is found that plastic compression starts at a lower stress ($-\sigma_c$) – a phenomenon known as the *Bauschinger Effect* (BE). The BE arises because, during the initial tensile plastic straining, internal stresses accumulate in the test-piece and oppose the applied strain. When the direction of straining is reversed these internal stresses now *assist* the applied strain, so that plastic yielding commences at a lower stress than that operating in tension.

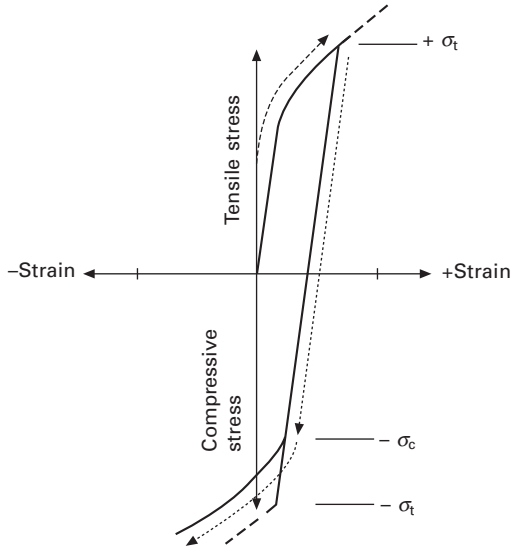

2.2 Illustration of the Bauschinger Effect when the direction of straining is reversed as indicated by the arrowed dotted line.

© Woodhead Publishing Limited, 2006

The BE may be encountered in the measurement of the yield strength of some linepipe steels. Tensile specimens are cut from the finished pipe and these are cold flattened prior to testing. The measured yield strength in such specimens can be significantly lower than that obtained on the (undeformed) plate from which the pipeline is manufactured. This is because the pipe has suffered compressive strain during the unbending process, so the tensile yield stress is reduced by the BE. The plate material thus has to be supplied with extra strength to compensate for this apparent loss in yield strength.

2.2.1 The behaviour of metals at larger strains

Figure 2.3 illustrates the form of a typical load–elongation curve for a ductile metal: after the initial elastic region, the gauge length of the specimen becomes plastic so that, if the load is reduced to zero, the specimen will remain permanently deformed. The load required to produce continued plastic deformation increases with increasing elongation, i.e. the material *work hardens*.

The volume of the specimen remains constant during plastic deformation, so as the gauge length elongates its cross-sectional area is progressively reduced. At first, work hardening more than compensates for this reduction in area and the gauge length elongates uniformly. The *rate* of work hardening decreases with strain, however, and eventually a point is reached when there is an insufficient increase in load due to work hardening to compensate for the reduction in cross-section, so that all further plastic deformation will be concentrated in this region and the specimen will undergo *necking*, with a progressive fall in the load. The onset of necking is known as *plastic instability*, and during the remainder of the test the deformation becomes localized until fracture occurs.

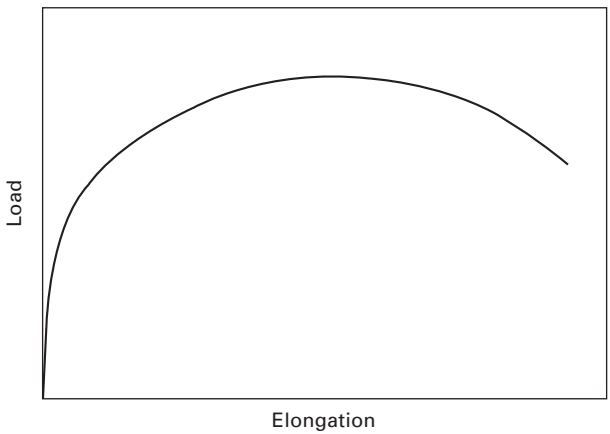

2.3 Tensile test of a ductile metal.

© Woodhead Publishing Limited, 2006

2.2.2 The engineering stress–strain curve

The load–elongation curve of Fig. 2.3 may be converted into the engineering stress–strain curve as shown in Fig. 2.4 The engineering, or conventional, stress σ is given by dividing the load (L) by the *original* cross-sectional area of the gauge length (A_o), and the strain (e) is as defined above, namely the extension of the gauge length ($l - l_o$) divided by gauge length (l_o).

The maximum conventional stress in Fig. 2.3 known as the *Ultimate Tensile Stress (UTS)* is defined as:

$$\text{UTS} = L_{max}/A_o$$

and this property is widely quoted to identify the strength of materials.

The tensile test also provides a measure of ductility. If the fractured test-piece is reassembled, the final length (l_f) and final cross-section (A_f) of the gauge length may be measured and the ductility expressed either as the engineering strain at fracture:

$$e_f = (l_f - l_o)/l_o,$$

or the reduction is cross-section at fracture, RA, where:

$$\text{RA} = (A_o - A_f)/A_o$$

These quantities are usually expressed as percentages. Because much of the plastic deformation will be concentrated in the necked region of the gauge length, the value of e_f will depend on the magnitude of the gauge length – the smaller the gauge length the greater the contribution to e_f from the neck itself. The value of the gauge length should therefore be stated when recording the value of e_f.

2.2.3 True stress–strain curve

The fall in the engineering stress after the UTS is achieved, due to the

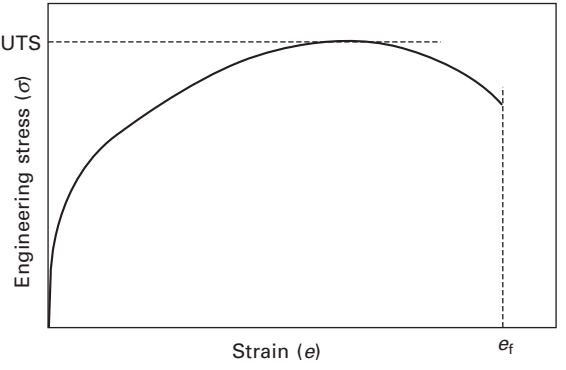

2.4 Engineering stress–strain curve.

© Woodhead Publishing Limited, 2006

presence of the neck, does not reflect the change in strength of the metal itself, which continues to work harden to fracture. If the *true stress*, based on the *actual* cross-section (A) of the gauge length, is used, the stress–strain curve increases continuously to fracture, as indicated in Fig. 2.5.

The presence of a neck in the gauge length at large strains introduces local triaxial stresses that make it difficult to determine the true longitudinal tensile stress in this part of the curve. Correction factors have to be applied to eliminate this effect.

Figure 2.5 illustrates the continued work hardening of the material until fracture, but, unlike the engineering stress–strain curve, the strain at the point of plastic instability and the UTS are not apparent. Their values may be readily obtained from Fig. 2.5 by the following approach:

At the UTS, the load (L) passes through a maximum, i.e. $\mathrm{d}L = 0$, and since $L = \sigma A$, we may write

$$\mathrm{d}L = \sigma\,\mathrm{d}A + A\,\mathrm{d}\sigma = 0$$

i.e. $$-\mathrm{d}A/A = \mathrm{d}\sigma/\sigma \qquad [2.1]$$

The volume of the gauge length ($V = Al$) is constant throughout the test ($\mathrm{d}V = 0$) and

$$\mathrm{d}l/l = -\mathrm{d}A/A \qquad [2.2]$$

Thus, from equations [2.1] and [2.2] we may write:

$$\mathrm{d}\sigma/\sigma = \mathrm{d}l/l \qquad [2.3]$$

But the strain, e, is defined as

$$e = (l - l_\mathrm{o})/\,l_\mathrm{o} = l/\,l_\mathrm{o} - 1 \qquad [2.4]$$

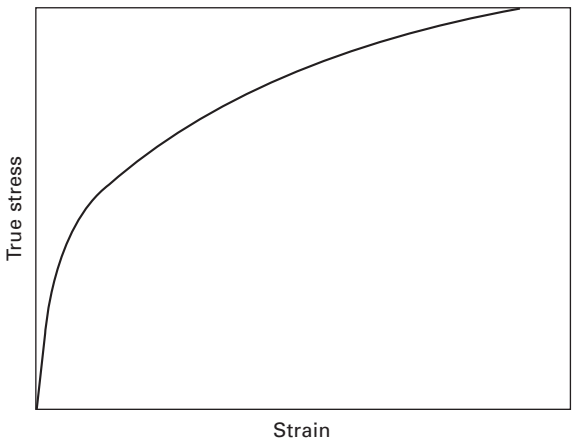

2.5 True stress–strain curve.

© Woodhead Publishing Limited, 2006

Therefore,

$$de = dl/l_o = (dl/l)(l/l_o) \quad [2.5]$$

So from [2.4] and [2.5] we obtain:

$$de = (dl/l)(1 + e) \quad [2.6]$$

Eliminating dl/l from [2.6] and [2.3] we find that, at the UTS:

$$d\sigma/de = \sigma_u/(1 + e_u) \quad [2.7]$$

where σ_u is the *true stress* at the UTS and e_u is the strain at the point of plastic instability. Equation [2.7] thus enables us to identify these values by means of the *Considère construction*, whereby a tangent to the true stress–strain curve is drawn from a point corresponding to –1 on the strain axis (Fig. 2.6). Additionally, the intercept of this tangent on the stress axis will give the value of the UTS, since

$$\sigma_u \text{ /UTS} = A_o/A = l/l_o \text{ (since the volume is constant)}$$

But from (2.4),

$$l/l_o = 1 + e$$

Thus, by similar triangles, it may be seen in Fig. 2.6 that the Considère tangent to the true stress–strain curve identifies both the point of plastic instability, the true stress at the UTS and the value of the UTS itself.

2.3 Bend testing

Testing brittle materials in tension is difficult, due to the problems of gripping the specimens in a tensile machine without breaking them. Furthermore, in

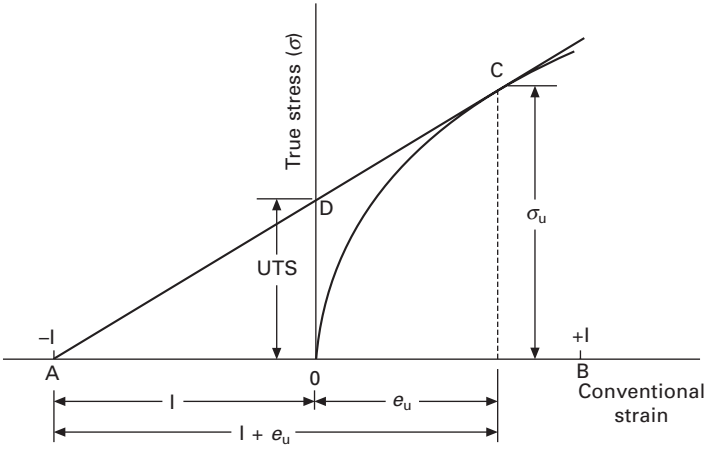

2.6 The Considère construction.

© Woodhead Publishing Limited, 2006

the case of materials such as glasses and ceramics, there is difficulty in shaping test-pieces of the 'dog-bone' shape without generating further flaws and defects in their surfaces.

Brittle materials are therefore frequently tested in bending in the form of parallel-sided bars, which are simple to make and may be deformed in either three-point or four-point bending (Fig. 2.7). In three-point bending the maximum tensile stress occurs at a point opposite the central load and in four-point bending the whole of the surface between the central loading edges, on the convex side of the bar, experiences the same maximum tensile stress. Provided that the spacing of the loading points is large compared with the depth of the bar and that the deflection of the bar is small, the maximum tensile surface stress is given by:

$$\sigma_{max} = M/D \qquad [2.8]$$

where M is the maximum bending moment (= $WL/4$ for 3-point and $Wd/2$ for 4-point loading) and D depends on the dimensions and shape of the cross-section of the bar. The $D = \frac{1}{4}\pi r^3$ for a circular cross-section and (breadth × depth^2)/6 for a rectangular section.

Because of the gradient of stress and strain through the cross-section of the specimen, from compressive on one side to tensile on the other, the apparent tensile strength values from a bend test tend to be higher than those from a tensile test. In brittle solids, the maximum tensile surface stress achieved in the test, given by equation [2.8], is referred to as the *flexural strength*, or the *modulus of rupture*.

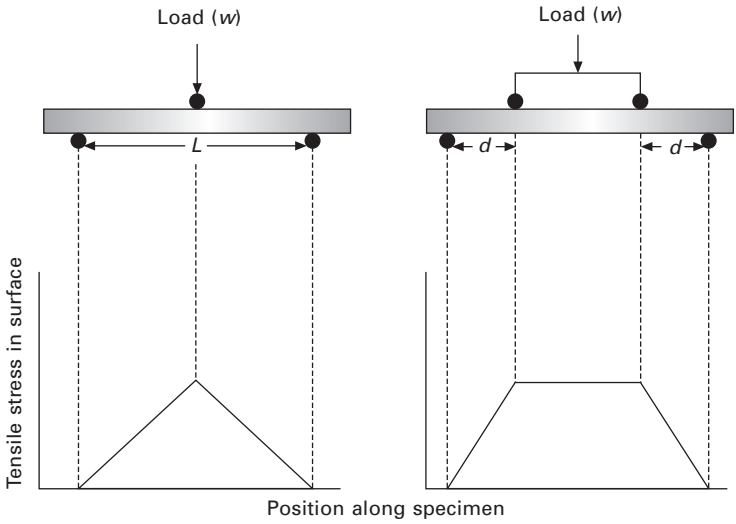

2.7 Geometry of (a) three- and (b) four-point bend tests showing the corresponding stress distributions in the specimen surface.

© Woodhead Publishing Limited, 2006

2.4 Statistics of brittle fracture

Since brittle solids fail by the propagation of pre-existing cracks under tension, measurement of their tensile strength will be subject to considerable experimental scatter. Ceramics and glasses contain a distribution of crack lengths, so it follows that there will be a statistical variation in their measured strengths. Furthermore, a large component will fail at a lower stress than a small one, since it is more likely that it will contain one of the larger cracks – so there is a volume dependence of the strength. Statistical models of strength are therefore needed in order to give a true prediction of the mechanical properties of brittle solids.

Weibull has defined the *survival probability*, $P_s(V)$, as the fraction of identical samples (each of volume V) which survive loading to a tensile stress σ, proposing the relation:

$$P_S(V) = \exp\left\{-\frac{V}{V_o}\left(\frac{\sigma}{\sigma_o}\right)^m\right\} \qquad [2.9]$$

where σ_o,V_o and m are constants, m being known as the *Weibull modulus*. The lower the value of m, the greater the variability of strength. The values of these constants are found by experiment: if the stress varies with position (as in the case of a bend test), then equation [2.9] can be integrated over the volume to give the appropriate design load.

2.5 Hardness testing

Hardness is not a well-defined property of materials and the tests employed assess differing combinations of the elastic, yielding and work-hardening characteristics. All the tests are essentially simple and rapid to carry out and are virtually non-destructive, so they are well-suited as a means of quality control. The hardness of materials has been assessed by a wide variety of tests, but we will confine ourselves to discussing two types of measurement – the resistance to *indentation* and the *height of rebound* of a ball or hammer dropped from a given distance.

2.5.1 Indentation hardness tests

There are two types of indentation hardness test. The first type (Brinell and Vickers) measures the size of the impression left by an indenter of prescribed geometry under a known load whereas the second type (Rockwell) measures the depth of penetration of an indenter under specified conditions.

© Woodhead Publishing Limited, 2006

2.5.2 The Brinell test

The surface of the material is indented by a hardened steel ball (whose diameter D is usually 10 mm) under a known load (L) (e.g. 3000 kg for steel) and the average diameter of the impression measured with a low-power microscope. The Brinell number (H_B) is the ratio of the load to the contact surface area of the indentation. Most machines have a set of tables for each loading force, from which the hardness may be read in units of kgf mm^{-2}.

If other sizes of indenter are used, the load is varied according to the relation: L/D^2 = constant in order to obtain consistent results. The constant is 30 for steel, 10 for copper and 5 for aluminium.

2.5.3 The Vickers test

A diamond square-based pyramid of 136° angle is used as the indenter, which gives geometrically similar impressions under differing loads (which may range from 5 to 120 kg). A square indent is thus produced, and the user measures the average diagonal length and again reads the hardness number (H_V) from the tables. The Brinell and Vickers hardness values are identical up to a hardness of about 300 kgf mm^{-2}, but distortion of the steel ball occurs in Brinell tests on hard materials, so that the test is not reliable above values of 600 kgf mm^{-2}.

For steels there is a useful empirical relationship between the UTS (in MPa) and H_V (in kgf mm^{-2}), namely:

$$\text{UTS} \approx 3.2\, H_V$$

2.5.4 The Rockwell test

Either a steel ball (Scale B) or a diamond cone (Scale C) is used and the indenter is first loaded with a minor load of 10 kg f, while the indicator for measuring the depth of the impression is set to zero. The appropriate major load is then applied and, after its removal, the dial gauge records the depth of the impression in terms of Rockwell numbers.

The correlation between the Rockwell, Vickers and Brinell Hardnesses is given in standard reference books and is indicated in Fig. 2.8.

It should be pointed out that, in the case of materials which exhibit time-dependence of elastic modulus or yield stress (for example, most polymers), the size of the indentation will increase with time, so the hardness value will depend on the duration of application of the load.

2.5.5 The Knoop test

The Knoop test uses a diamond pyramidal indenter of apex angles 130° and

© Woodhead Publishing Limited, 2006

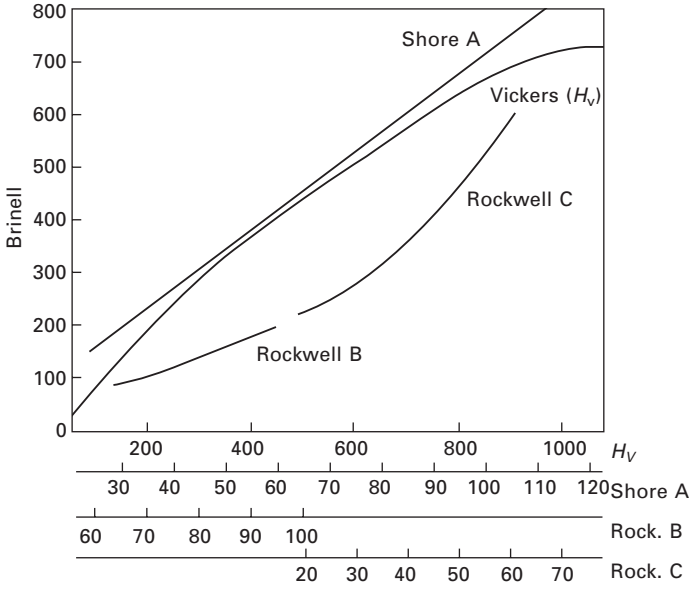

2.8 Relation between various scales of hardness.

172.5°, thus giving a rhombohedral impression with one diagonal (L) being 7 × longer than the other and with a depth which is one thirtieth of L. It is particularly useful for measuring the relative hardnesses of brittle materials, such as glasses and ceramics, when lower loads (P) are employed than in the Vickers test.

The Knoop Hardness Number (KHN, in kgf mm^{-2}) is given by the relation:

$$\text{KHN} = 14.229P/L^2$$

2.5.6 The Shore scleroscope

A small diamond-pointed hammer weighing 2.5 g falls freely from a standard height down a graduated glass tube. The height of the first rebound is taken as the index of hardness and this simple apparatus may be readily transported for testing rolls, gears, etc. *in situ*. Its correlations with the indentation hardness techniques are also shown in Fig. 2.8.

The Shore test may also be employed to measure the elastic response of elastomers, as a check of the degree of cross-linking.

2.6 Fracture toughness testing

The *toughness* of a material must be distinguished from its *ductility*. It is true that ductile materials are frequently tough, but toughness combines both strength and ductility, so that some soft metals like lead are too weak to be

© Woodhead Publishing Limited, 2006

tough whereas glass-reinforced plastics are very tough although they exhibit little plastic strain.

One approach to toughness measurement is to measure the work done in breaking a specimen of the material, such as in the Charpy-type of impact test. Here a bar of material is broken by a swinging pendulum and the energy lost by the pendulum in breaking the sample is obtained from the height of the swing after the sample is broken. A serious disadvantage of such tests is the difficulty of reproducibility of the experimental conditions by different investigators, so that impact tests can rarely be scaled up from laboratory to service conditions and the data obtained cannot be considered to be true material parameters.

Fracture toughness is now assessed by establishing the conditions under which a sharp crack will begin to propagate through the material and a number of interrelated parameters may be employed to express this property. To introduce these concepts, we will first consider the *Griffith criterion* for the brittle fracture of a linear elastic solid in the form of an infinite plate of unit thickness subjected to a tensile stress σ, which has both ends clamped in a fixed position. This is a condition of *plane stress*, where all stresses are acting in the plane of the plate. The elastic energy stored per unit volume is given by the area under the stress–strain curve, i.e. 1/2 stress × strain which may be written:

$$\text{Stored elastic energy} = \sigma^2/2E \text{ per unit volume}$$

where E is Young's modulus.

If a crack is introduced perpendicular to σ and the length of the crack ($2c$) is small in comparison with the width of the plate, some relief of the elastic stress will take place. Taking the volume relieved of stress as a cylindrical volume of radius c (Fig. 2.9), then the elastic energy (U_v) released in creating the crack is:

$$U_v = (\pi c^2)(\sigma^2/2E)$$

in a uniform strain field, but is twice this if the true strain field is integrated to obtain a more accurate result, i.e.

$$U_v = \pi c^2 \sigma^2/E \qquad [2.10]$$

Griffith's criterion states that, for a crack to grow, the release of elastic strain energy due to that growth has to be greater than the surface energy of the extra cracked surfaces thus formed. In Fig. 2.9, the area of crack faces is $4c$, so, if the surface energy of the material is γ per unit area, then the surface energy (U_s) required is,

$$U_s = 4c\gamma \qquad [2.11]$$

Figure 2.10 represents energy versus crack length and it is analogous to

© Woodhead Publishing Limited, 2006

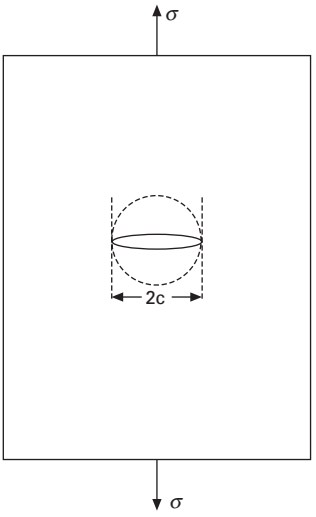

2.9 Crack in plate of unit thickness.

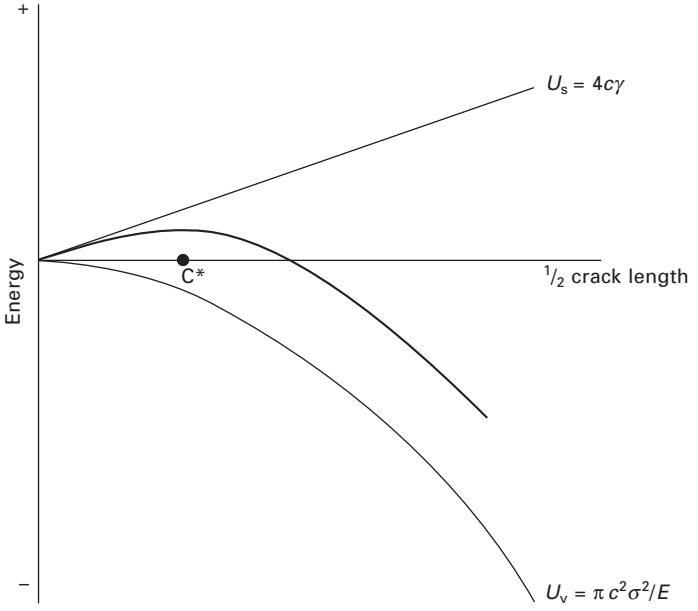

2.10 Change in energy with crack length.

the diagram of free energy change versus embryo size in the theory of nucleation of phase transformations (Fig. 1.4). The critical crack size c^* is thus when:

© Woodhead Publishing Limited, 2006

$$d/dc\ (4c\gamma - \pi c^2\sigma^2/E) = 0$$

i.e. $$2\gamma = \pi c^*\sigma^2/E$$

so $$\sigma = (2E\gamma/\pi c^*)^{1/2} \quad [2.12]$$

which is the well-known Griffith equation. At stress σ, cracks of length below $2c^*$ will tend to close and those greater than $2c^*$ will grow. Thus, at a given stress level, there is a critical flaw size which will lead to fracture and, conversely, for a crack of a given length, a critical threshold stress is required to propagate it.

Under conditions of *plane strain*, [2.12] becomes:

$$\sigma = [2E\gamma/\pi(1 - \nu^2)c^*]^{1/2} \quad [2.13]$$

where ν is the Poisson ratio for the material.

In considering real materials, rather than an ideal elastic solid, the work required to create new crack surfaces is more than just the thermodynamic surface energy, 2γ. Other energy absorbing processes, such as plastic deformation, need to be included and these are taken into account by using the *toughness*, G_c, to replace 2γ in equations [2.12] and [2.13] giving a fracture stress σ_F:

$$\sigma_F = (E\ G_c/\alpha\pi c)^2 \quad [2.14]$$

where α = unity in plane stress, and $(1 - \nu^2)$ in plane strain.

A related measure of toughness is the *fracture toughness*, K_c, which is related to G_c by:

$$G_c = \alpha K_c^2 / E \quad [2.15]$$

From equation [2.14] this may be written:

$$K_c = \sigma_F\ (\pi c)^2 \quad [2.16]$$

The fracture toughness is measured by loading a sample containing a deliberately introduced crack of length $2c$, recording the tensile stress σ_c at which the crack propagates. This is known *crack opening*, or *mode I* testing. The toughness K_c is then calculated from

$$K_c = Y\sigma_c\ (\pi c)^2 \quad [2.17]$$

where Y is a geometric factor, near unity, which depends on the details of the sample geometry. The toughness can then be obtained by using equation [2.15].

This approach gives well-defined values for K_c and G_c for brittle materials (ceramics, glasses and many polymers), but, in ductile metals, a *plastic zone* develops at the crack tip. The linear elastic stress analysis we have assumed so far can be applied only if the extent of plasticity is small compared with the specimen dimensions. Additionally, the testpiece must be sufficiently

© Woodhead Publishing Limited, 2006

thick in order that most of the deformation occurs under conditions of *plane strain*. Figure 2.11 illustrates the effect of specimen thickness on the measured value of the fracture toughness, K_c: the fracture toughness can be halved as the stress conditions change from plane stress to plane strain with increasing specimen thickness. Once under plane strain, however, the value of the toughness becomes independent of the thickness and this value is referred to as K_{Ic}, and is regarded as a material parameter. The corresponding value of G_{Ic} may be calculated from equation [2.15].

The two requirements of a relatively small plastic zone and plane strain conditions impose conditions upon the test-piece dimensions which have to be fulfilled in valid fracture toughness tests. These dimensions are always stated in the appropriate testing standards, e.g. BS 7448 (1991).

In circumstances of extensive plasticity, an alternative toughness parameter has been proposed, namely the *crack tip opening displacement (CTOD)*, usually given the symbol δ. The CTOD is obtained from the reading of a clip-gauge placed across the crack mouth and, under conditions of fracture, a critical value of δ_c is determined. If the yield stress of the material is σ_y, the toughness may then be obtained from the relation:

$$G_c = \sigma_y \delta_c \qquad [2.18]$$

2.6.1 The *J* integral

There are types of material, e.g. elastomers, which behave in a *non-linear* elastic manner, i.e. their reversible stress–strain graph is curved. The energy

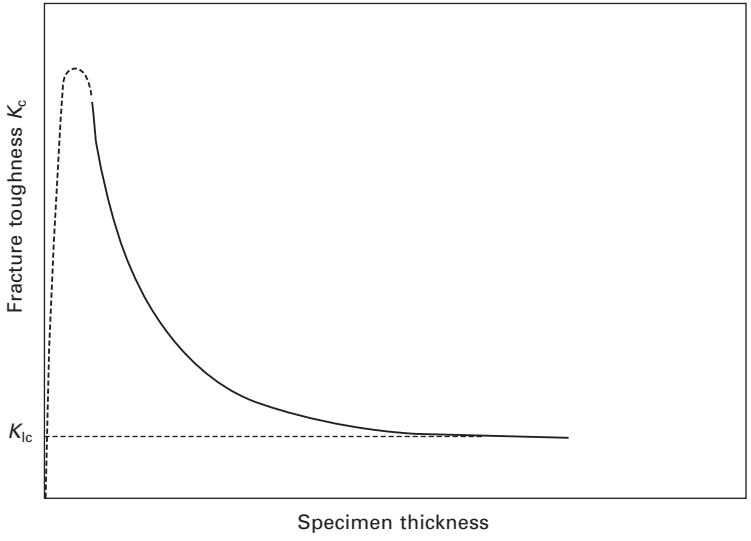

2.11 Change in fracture toughness with specimen thickness.

© Woodhead Publishing Limited, 2006

release rate for such materials is characterized by a parameter termed J, which is the non-linear equivalent of the potential energy release rate G per unit thickness derived above. In a linear elastic material, J would be identical to G and the reader is directed to the British Standard BS 7448:1991, which describes methods for the determination of K_{Ic}, critical CTOD and critical J values of metallic materials.

2.7 Time-dependent mechanical properties

We will now consider some material properties whose values are time-dependent, namely:

Creep, which refers to slow plastic deformation with time under load;
Superplasticity, whereby certain metals, alloys, intermetallics and ceramics can be made to deform at elevated temperatures to very large strains in tension: elongations of 200–500% are quite common;
Fatigue, which is the damage and failure of materials under cyclic load;
Environment-assisted cracking in which cracks propagate under the *combined* action of an applied stress and an aggressive environment; and finally
Time-dependent elastic properties, which appears as *viscoelastic behaviour* in polymers and, under conditions of cyclic loading of solids in general, as the *damping capacity*, which measures the degree to which a material dissipates vibrational energy.

2.7.1 Creep

Creep occurs when materials are loaded above about $^1/_3T_m$. Tests are normally conducted under uniaxial tensile stress on a specimen similar to that used in tensile testing, and the test-piece and pull-rods may be situated in a tubular furnace, whose temperature is accurately controlled. The strain in the specimen is monitored by a sensitive extensometer and typical tensile strain–time curves are shown in Fig. 2.12 for such experiments.

In curve A, after the initial instantaneous extension, a regime of decreasing creep-rate occurs (*primary creep). Secondary creep* occurs at an approximately constant rate, sometimes referred to as the *minimum creep rate*, which is followed by an accelerating regime of *tertiary creep*, leading to rupture.

Curve B illustrates the type of result obtained if the test is conducted at a lower stress or lower temperature: only primary creep is observed and fracture may not occur in the duration of the test. Curve C shows the effect of higher stresses or temperatures: secondary creep may be absent and early failure may occur.

Returning to the general form of curve A in Fig. 2.12, the minimum creep rate $(\dot{\varepsilon})$ under stress σ and temperature T may be characterized by the creep constants, $\dot{\varepsilon}_0$, σ_o, n and Q in the equation:

© Woodhead Publishing Limited, 2006

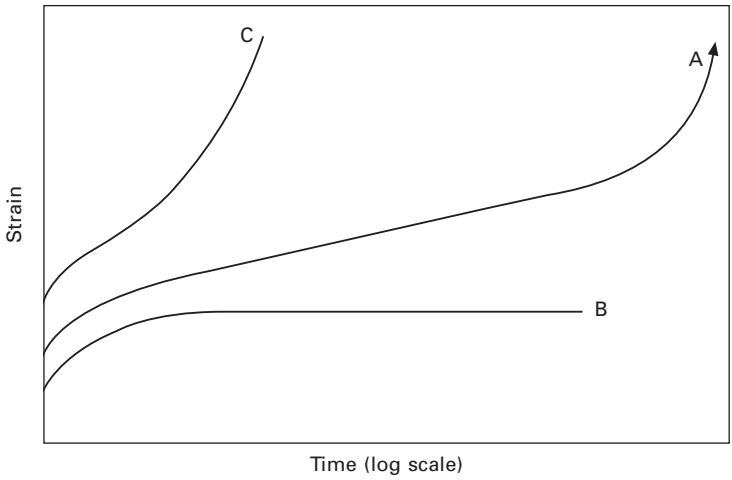

2.12 Showing various strain–time curves for creep.

$$\dot{\varepsilon} = \dot{\varepsilon}_0 (\sigma/\sigma_o)^n \exp - (Q/RT) \quad [2.19]$$

Considerable time and thus expense is involved in determining creep data in this form, and design data are often given as a series of curves relating stress and time at a given test temperature to produce a given constant creep strain (1%, 2%, etc.) or time to rupture (or 'creep life'), both are shown in the example in Fig. 2.13 for a nickel-based alloy in single crystal form (due to W. Schneider, J. Hammer and H. Mughrabi, in *Superalloys 1992*, edited by S.D. Antolovich *et al.*, TMS, Warrendale, PA, 1992, 589).

Acquisition of creep life data requires no strain measurement to be carried out, but it clearly can given no indication of the time spent in the various stages of the creep curve. Engineering components may thus be designed on

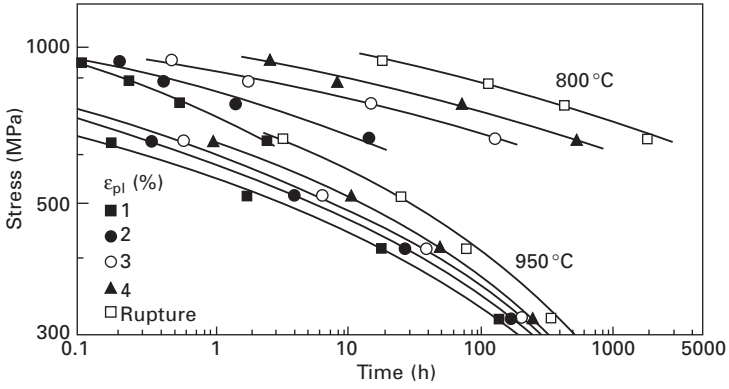

2.13 Creep–rupture diagrams for a single crystal Ni-based superalloy (CMSX-4) for 800 and 950 °C.

© Woodhead Publishing Limited, 2006

a knowledge of the stresses which the relevant materials can withstand without fracture in times up to the anticipated service life. In the case of components for chemical and electricity generating plant, designs are generally based on the 100 000 hour rupture data, although economic benefits would obviously be derived if lives could be extended to, say, 250 000 hours.

For alloy development and production control, relatively short term creep tests are employed. Where a component experiences creep for very protracted periods, however, design data must itself be acquired from very lengthy tests rather than by extrapolation, since structural changes may occur in the material under these circumstances. Problems may also be encountered because the mechanisms of deformation and fracture may differ in different regimes of stress and temperature. With a limited number of materials, however, methods of extrapolating empirical data have been successfully developed for both creep strain and stress-rupture properties, allowing data for times of 10 years or more to be estimated from high-precision creep curves obtained in times of three months or less.

For further information on this topic, the reader is referred to 'Creep of Metals and Alloys' by R.W. Evans and B. Wilshire (The Institute of Materials, London, 1985).

2.7.2 Superplasticity

In general, a superplastic material exhibits at a given temperature a high strain-rate sensitivity (m), which may be represented by the relation:

$$\sigma = K\dot{\varepsilon}^m \qquad [2.20]$$

where σ is the flow stress, and $\dot{\varepsilon}$ the strain rate. The large neck-free elongation during superplasticity comes from the resistance to necking in certain microstructural and deformation conditions. The influence of the strain rate sensitivity parameter on promoting large ductility can be understood by considering the change in cross-section area with time during a tensile test:

$$\frac{\mathrm{d}A}{\mathrm{d}t} = -\left(\frac{P}{K}\right)^{1/m} A^{(m-1)/m} \qquad [2.21]$$

where A is the cross section area, t is the time, P is the load and K is the temperature and structure-dependent parameter in equation [2.20]. For m = 1, the change in cross-section area becomes independent of A, a reason for the large ductility exhibited by glass at elevated temperature.

Crystalline materials exhibit m = 1 at very slow strain rates, which is not considered practical for forming processes. A value of m = 0.5 leads to diffuse necking and thus to high elongations to failure. However, dA/dt also depends on the value of P and the fact that loads during the deformation of

© Woodhead Publishing Limited, 2006

fine-grained materials at elevated temperatures are low is an additional factor leading to a large elongation. The grain-size dependence of the steady-state strain rate at elevated temperatures may be expressed in an equation in the same form as that equation [2.19]:

$$\dot{\varepsilon} = (ADGb/kT)(b/d)^{p}(\sigma/G_{o})^{n} \quad [2.22]$$

where A is a dimensionless constant, D is the appropriate diffusion coefficient, G is the shear modulus, b the magnitude of the Burgers vector (see Chapter 3), k is Boltzmann's constant, d is the grain size, and p is the inverse grain size exponent.

In accordance with this relationship, the principal requirements for a superplastic material are (a) a fine and equiaxed grain size (<10 μm for metals and <1 μm for ceramics) that is reasonably stable during deformation, (b) a temperature that is more than about one half the melting point of the matrix (in degrees K), and (c) a strain rate that is typically between 10^{-2} s^{-1} and 10^{-6} s^{-1}.

Superplastic materials are thus multi-phase, which promotes pinning of the grain boundaries during the high-temperature forming process, hence inhibiting grain growth. Titanium and aluminium alloys have been developed for industrial superplastic forming and it is also an accepted forming method for producing the vanes of gas turbine engines using certain nickel-based superalloys. With further refinement of grain size, superplasticity can be extended to significantly higher (and hence commercially desirable) strain rates.

2.7.3 Fatigue

The progression of fatigue damage can be classified into a number of stages involving (a) the nucleation of microscopic cracks, (b) their growth and coalescence and (c) the propagation of a macroscopic crack until failure. The original approach to fatigue design involved characterizing the *total fatigue life* to failure of initially uncracked testpieces in terms of the number of applications of a cyclic stress range (the S–N curve in 'high-cycle fatigue') or a cyclic strain range ('low-cycle fatigue').

The S–N curve

Smooth, unnotched testpieces are prepared, carefully avoiding sharp changes in cross-section that may give rise to stress concentrations. Testing machines apply fluctuating loads in tension, compression, torsion, bending, or combinations of such loads, and the number of cycles to specimen failure is recorded. Test methods are described in detail in the ASTM Standards E466–E468.

© Woodhead Publishing Limited, 2006

Figure 2.14 illustrates a typical stress pattern, the *stress range* ($\Delta\sigma = \sigma_{max} - \sigma_{min}$) and the *mean stress* [$\sigma_m = (\sigma_{max} + \sigma_{min})/2$] being indicated, as well as the *cyclic stress amplitude* ($\sigma_a = \Delta\sigma/2$). The mean stress may be zero, tensile or compressive in nature, and typical test *frequencies* employed depend on the machine design – whether it is actuated mechanically or servo-hydraulically for example – but are typically in the range 10–100 Hz.

The data from such tests are usually plotted upon logarithmic axes, as illustrated in the S–N curve of Fig. 2.15. Because of the protracted time involved, tests are seldom conducted for more than 5×10^7 or 10^8 cycles, and the curves may be of two types – those showing a continuous decline and those showing a horizontal region at lives greater than about 10^6 cycles. The horizontal line thus defines a stress range below which the fatigue life is infinite and this is defined as the *endurance limit* or *fatigue limit*. The majority

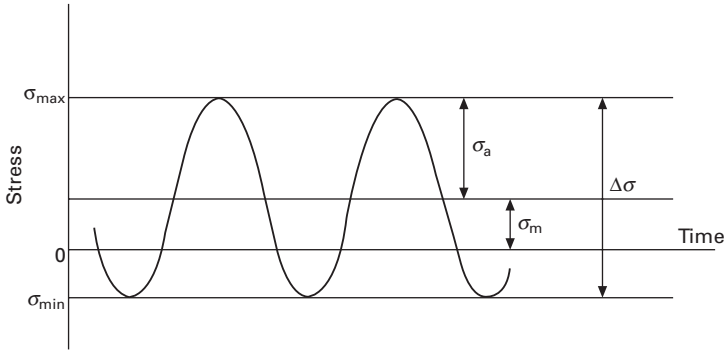

2.14 Typical stress pattern in fatigue.

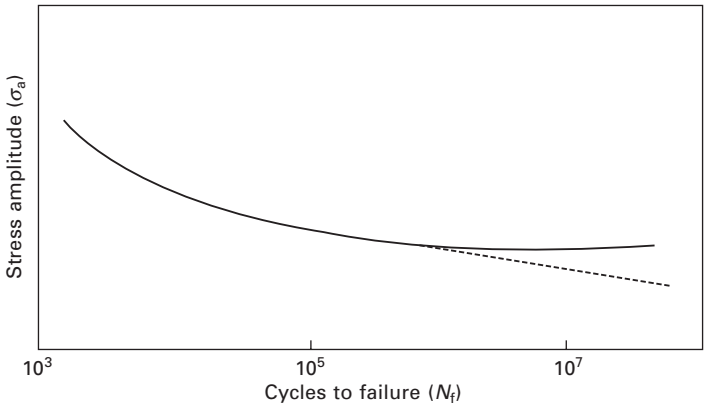

2.15 Typical S–N diagram showing the variation of the stress amplitude for fully reversed fatigue loading as a function of the number of cycles to failure for ferrous alloys (continuous line) and nonferrous alloys (dotted line).

© Woodhead Publishing Limited, 2006

of materials do not exhibit an endurance limit, although the phenomenon is encountered in many steels and a few aluminium alloys.

The curve may be described by:

$$\sigma_a = \sigma'_f (2N_f)^b \quad [2.23]$$

where σ'_f is the fatigue strength coefficient (which is roughly equal to the fracture stress in tension) and b the fatigue strength exponent or *Basquin exponent*. For most metals $b \approx -0.1$; some values of b and of σ'_f for a number of engineering alloys are given in Table 2.1.

Mean stress effects on fatigue life

The mean level of the imposed stress cycle (Fig. 2.14) influences the fatigue life of engineering materials: a decreasing fatigue life is observed with increasing mean stress value. The effect can be modelled by *constant life diagrams*, Fig. 2.16. In these models, different combinations of the mean stress and the stress range are plotted to provide a constant (chosen) fatigue life. For that life, the fatigue stress range for fully reversed loading ($\sigma_m = 0$) is plotted on the vertical axis at σ_{fo} and the value of the yield strength σ_y and the UTS of the material is marked on the horizontal axis. The Goodman model predicts that, as the mean stress increases from zero, the fatigue stress for that life (σ_{fm}) decreases linearly to zero as the mean stress increases to the UTS, i.e.:

$$\sigma_{fm} = (1 - \sigma_m/\text{UTS}) \quad [2.24]$$

The Goodman relation matches experimental observation quite closely for brittle metals, whereas the Gerber model, which matches experimental observations for ductile alloys, predicts a parabolic decline in fatigue stress with increasing mean stress:

$$\sigma_{fm} = [1 - (\sigma_m/\text{UTS})^2] \quad [2.25]$$

Table 2.1 Some cyclic strain-life data (C. C. Osgood, *Fatigue Design*, New York, Pergamon Press, 1982)

Material	Condition	σ_y (MPa)	σ'_f (MPa)	ε'_f	b	c
Pure Al (1100)	Annealed	97	193	1.80	–0.106	–0.69
Al–Cu (2014)	Peak aged	462	848	0.42	–0.106	–0.65
Al–Mg (5456)	Cold worked	234	724	0.46	–0.110	–0.67
Al–Zn–Mg (7075)	Peak aged	469	1317	0.19	–0.126	–0.52
0.15%C steel (1015)	Normalized	228	827	0.95	–0.110	–0.64
Ni–Cr–Mo steel (4340)	Quenched and tempered	1172	1655	0.73	–0.076	–0.62

© Woodhead Publishing Limited, 2006

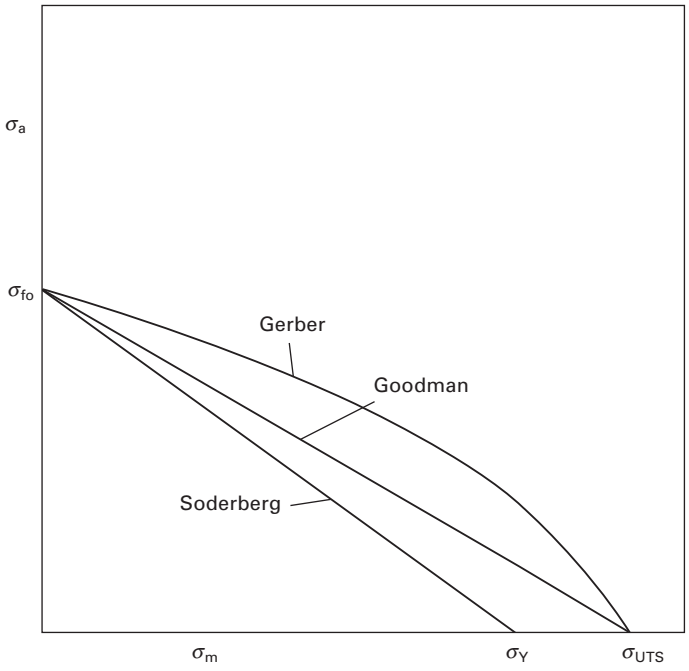

2.16 Models relating mean stress to fatigue stress range.

The Soderberg model, which provides a conservative estimate of fatigue life for most engineering alloys, predicts a linear decrease in the fatigue stress with increasing mean stress up to σ_y:

$$\sigma_{fm} = (1 - \sigma_m/\sigma_y) \qquad [2.26]$$

Low-cycle fatigue

The stresses associated with low-cycle fatigue are generally high enough to cause appreciable plastic deformation before fracture and, in these circumstances, the fatigue life is characterized in terms of the *strain range*. Coffin (1954) and Manson (1954) noted that when the logarithm of the plastic strain amplitude, $\Delta\varepsilon_p/2$, was plotted against the logarithm of the number of load reversals to failure, $2N_f$, for metallic materials, a linear result was obtained, i.e.

$$\Delta\varepsilon_p/2 = \varepsilon_f'(2N_f)^c \qquad [2.27]$$

where ε_f' is the fatigue ductility coefficient and c the fatigue ductility exponent.

The *total* strain amplitude $\Delta\varepsilon/2$ is the sum of the elastic strain amplitude $\Delta\varepsilon_e/2$ and $\Delta\varepsilon_p/2$, but

© Woodhead Publishing Limited, 2006

$$\Delta\varepsilon_e/2 = \Delta\sigma/2E = \sigma_a/E$$

where E is Young's modulus.

Thus, using equation [2.23] we obtain:

$$\Delta\varepsilon_e/2 = \sigma'_f/E(2N_f)^b \quad [2.28]$$

and combining equations [2.23] and [2.27] we can write the total strain amplitude:

$$\Delta\varepsilon/2 = \sigma'_f/E(2N_f)^b + \varepsilon'_f(2N_f)^c \quad [2.29]$$

Equation [2.29] forms the basis for the strain-life approach to fatigue design, and Table 2.1 gives some strain-life data for some common engineering alloys.

Fatigue crack growth – the use of fracture mechanics

The total fatigue life discussed so far is composed of both the crack nucleation and crack propagation stages. *Defect-tolerant* design, however, is based on the premise that engineering structures contain flaws and that the life of the component is the number of cycles required to propagate the dominant flaw – taken to be the largest undetectable crack size appropriate to the particular method of non-destructive testing employed.

Fracture mechanics may be employed to express the influence of stress, crack length and geometrical conditions upon the rate of fatigue crack propagation. Thus, by employing equation (2.17), a stress range $\Delta\sigma$ applied across a surface crack of length a, will exert a *stress intensity range*, ΔK, given by:

$$\Delta K = Y\Delta\sigma\pi a)^{\frac{1}{2}} \quad [2.30]$$

where Y is the geometrical factor.

Pre-cracked test-pieces may thus be tested under fluctuating stress and the growth of the crack continuously monitored, for example by recording the change in resistivity of the specimen. After calibration, the resistivity changes may be interpreted in terms of changes in crack length and the data may be plotted in the form of crack growth per cycle (da/dN) versus ΔK curves. Figure 2.17 illustrates schematically the form of crack growth curve obtained in the case of ductile solids.

For most engineering alloys, the curve is seen to be essentially sigmoidal in form. Over the central, linear, portion (regime B in Fig. 2.17) the fatigue crack growth rate (FCGR) is observed to obey the Paris power law relationship:

$$da/dN = C(\Delta K)^m \quad [2.31]$$

where C and m are constants.

© Woodhead Publishing Limited, 2006

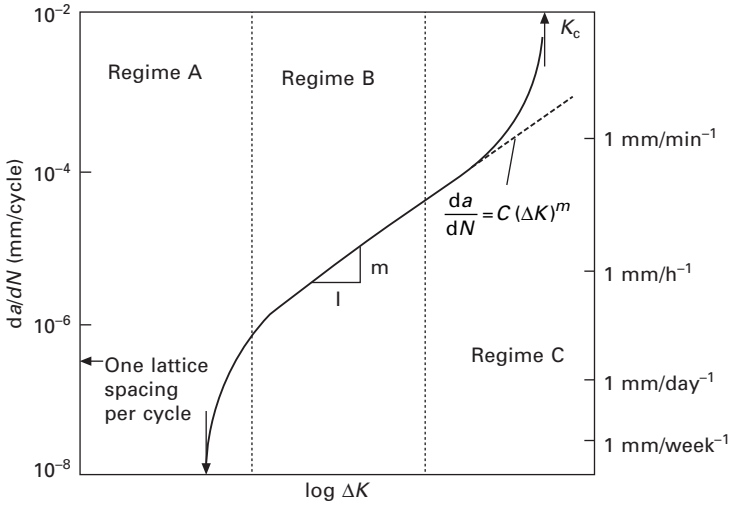

2.17 Schematic illustration of fatigue crack growth curve.

For tensile fatigue, ΔK refers to the range of mode I stress intensity factors in the stress cycle, i.e.

$$\Delta K = K_{max} - K_{min}, \text{ and } K_{min}/K_{max} \text{ is known as } R, \text{ the } \textit{load ratio}.$$

In the Paris regime, the FCGR is, in general, insensitive to microstructure of the material and to the value of R.

In regime A, the average FCGR becomes smaller than a lattice spacing, suggesting the existence of a threshold stress intensity factor range, ΔK_{th}, below which the crack remains essentially dormant. The value of ΔK_{th} is not a material constant, however, but is highly sensitive to microstructure and also to the value of R, as apparent in the data for a variety of engineering alloys shown in Fig. 2.18: at high mean stress (high R), lower thresholds are encountered.

In regime C, FCG rates increase rapidly to final fracture. This corresponds to K_{max} in the fatigue cycle achieving the fracture toughness, K_c, of the material. As indicated in Fig. 2.17, this regime is again sensitive to the value of R.

Fatigue charts

Fleck, Kang and Ashby (*Acta Metall. Mater.*, 1994, **42**, 365–381) have constructed some material property charts for fatigue analogous to that illustrated in Fig. 0.1 which relates modulus to density of engineering materials. They are useful in showing fundamental relationships between fatigue and static properties, and in selecting materials for design against fatigue. Thus, Fig. 2.19 shows the well-known fact that the endurance limit σ_e increases in

© Woodhead Publishing Limited, 2006

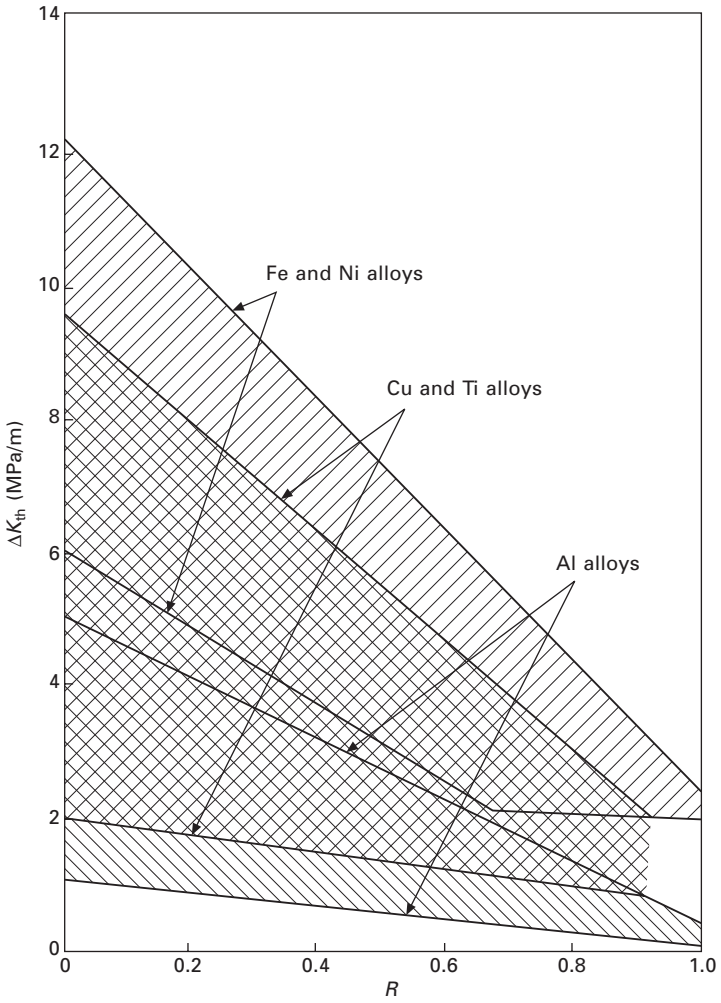

2.18 Ranges of threshold ΔK versus load ratio (R) for some engineering alloys.

a roughly linear way with the yield stress σ_y. The *fatigue ratio*, defined as σ_e/σ_y at $R = -1$, appears as a set of diagonal lines. The ratio is almost 1 for engineering ceramics, about 0.5 for metals and elastomers, and about 0.3 for polymers, foams and wood.

Figure 2.20 refers to the behaviour of cracked specimens and charts the relationship between the fatigue threshold and the fracture toughness of materials. The correlation between ΔK_{th} and K_{Ic} is less good than between σ_e and σ_y, reflecting the fact that, with the exception of polymers and woods, cracked materials are more sensitive to fatigue loading than those which are initially uncracked. The ratios shown in Fig. 2.19 and 2.20 vary widely with

© Woodhead Publishing Limited, 2006

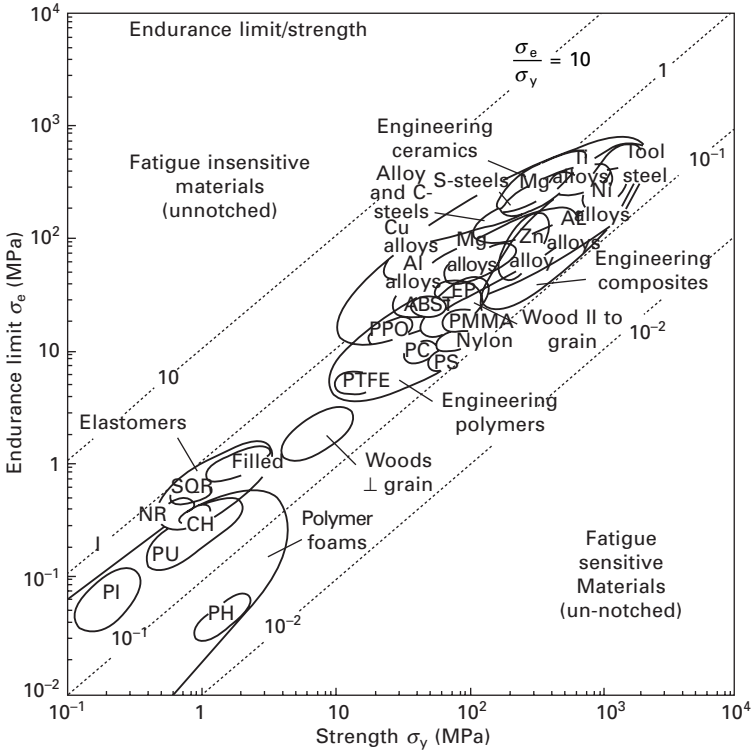

2.19 Endurance limit versus yield strength for engineering materials.

material class, which emphasizes the importance of employing fatigue properties rather than monotonic properties in design for cyclic loading.

2.7.4 Environment-assisted cracking

Materials are known to fail under stress when the *initial* stress intensity level is considerably below K_{Ic}. This is because cracks are able to grow to a critical size until the stress intensity level is increased to the critical value. There are a number of processes which may give rise to such crack extension in the presence of an applied static stress in an aggressive environment, namely *stress-corrosion cracking (SCC)*, *hydrogen embrittlement (HE)* and *liquid metal embrittlement (LME)*. These phenomena are referred to collectively as *environment-assisted cracking (EAC)*.

d*a*/d*t* – *K curves*

The EAC effect is encountered in polymers, ceramics and metallic materials. In order to quantify EAC processes, the rate of crack advance (d*a*/d*t*) is

© Woodhead Publishing Limited, 2006

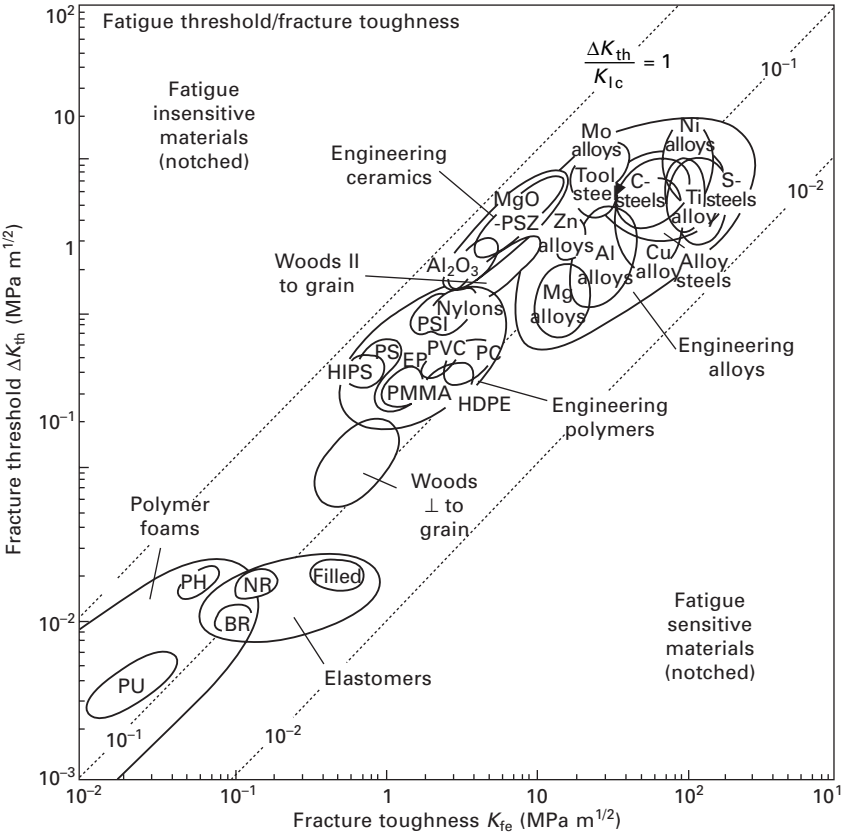

2.20 Threshold stress intensity range versus fracture toughness of engineering materials.

monitored as a function of the instantaneous value of the stress intensity. Cracked specimens are tested in Mode I (crack opening mode) and, in general, the data are represented on plots of log da/dt versus K in the form shown schematically in Fig. 2.21.

Three distinct crack growth regimes are shown (though all may not be present in a given material). In region I, da/dt is strongly dependent on K and, in some materials, the slope of this part of the curve is so steep that a value $K_{\mathrm{I\,EAC}}$ may be defined, i.e. a level of K_{I} below which da/dt becomes vanishingly small.

In region II, the rate of crack growth appears to be relatively independent of the prevailing level of K. The crack extension rate is still strongly dependent on the temperature, pressure and the environment, however. Finally, in region III, da/dt is strongly K-dependent and, eventually, the crack grows unstably as K approaches K_{Ic}.

© Woodhead Publishing Limited, 2006

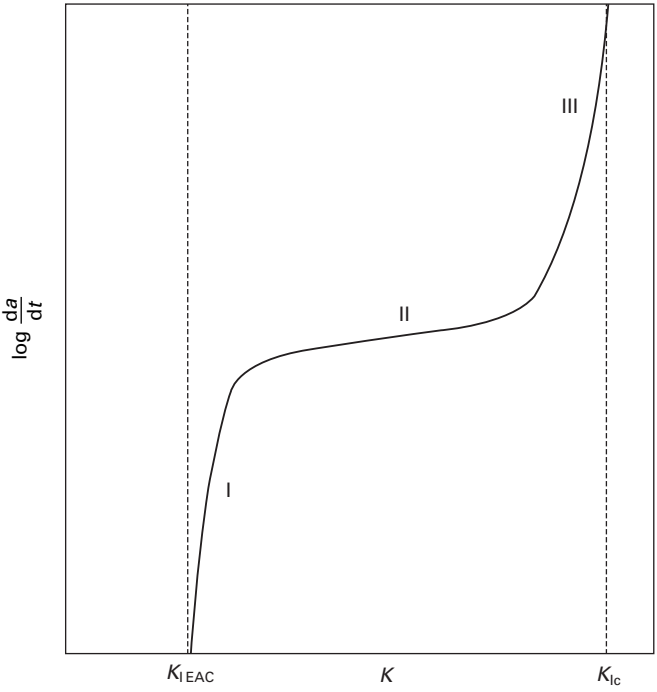

2.21 Diagram showing three stages of environment-assisted cracking under sustained loading in an aggressive atmosphere. Lower and upper K limits of plot determined by $K_{I\,EAC}$ and K_{Ic}, respectively.

2.7.5 Time-dependent elastic properties

Vibrating solids

If a material is loaded elastically to a stress σ, the stored elastic energy per unit volume is:

$$U = \int_0^{\sigma_{max}} \sigma \mathrm{d}e$$

If it is loaded and then unloaded it dissipates an energy

$$\Delta U = \oint \sigma \mathrm{d}e$$

The *specific damping capacity D* is defined by the ratio:

$$D = \Delta U/U \qquad [2.32]$$

Another measure of damping is the *logarithmic decrement* δ which is the log of the ratio of successive amplitudes of natural vibration of the solid. The effect arises because the elastic forces acting may also assist thermal energy

© Woodhead Publishing Limited, 2006

fluctuations to bring about atom movements, which are also time-dependent. The effect of these movements is to bring about time-dependent relaxations of stress in the lattice, an effect known as *anelasticity*, and each relaxation process has its own characteristic *time constant*. If, therefore, the damping is measured as a function of frequency of cyclic loading, a spectrum may be obtained with damping peaks occurring at characteristic frequencies, giving information about the molecular or atomic processes causing the loss or energy absorbing peaks.

The value of δ is very easily measured, for example by employing the sample as a torsion pendulum. The logarithmic decrement usually has a very low value in metals, but it can rise to high values in polymers, with peaks occurring in the region of the so-called *glass-transition temperature*. In this temperature range, long-range molecular motion is hindered and damping is great.

Viscoelastic behaviour of polymers

We have seen in Chapter 1 that a thermoplastic polymer consists of a random mass of molecular chains, retained by the presence of secondary bonds between the chains. Under load, the chains are stretched and there is a continuous process of breaking and remaking of the secondary bonds as the polymer seeks to relax the applied stress. At low strains, this anelastic behaviour is reversible in many plastics and the laws of *linear viscoelasticity* are obeyed.

The linear viscoelastic response of polymeric solids has been described by a number of mechanical models which provide a useful physical picture of time-dependent deformation. These models consist of combinations of *springs* and *dashpots*. A spring element describes linear elastic behaviour:

$$\varepsilon = \sigma/E \quad \text{and} \quad \gamma = \tau/G$$

where γ is the shear strain, τ the shear stress and G the shear modulus. A dashpot consists of a piston moving in a cylinder of viscous fluid, and it describes viscous flow:

$$\dot{\varepsilon} = \sigma/\eta \quad \text{and} \quad \dot{\gamma} = \tau/\eta$$

where $\dot{\varepsilon}$ and $\dot{\gamma}$ are the tensile and shear strain rates and η is the fluid viscosity, which varies with temperature according to:

$$\eta = A \exp(\Delta H/RT)$$

where A is a constant, and ΔH is the viscous flow activation energy.

Maxwell model

If the spring and dashpot are in series (Fig. 2.22(a)), the stress on each is the

© Woodhead Publishing Limited, 2006

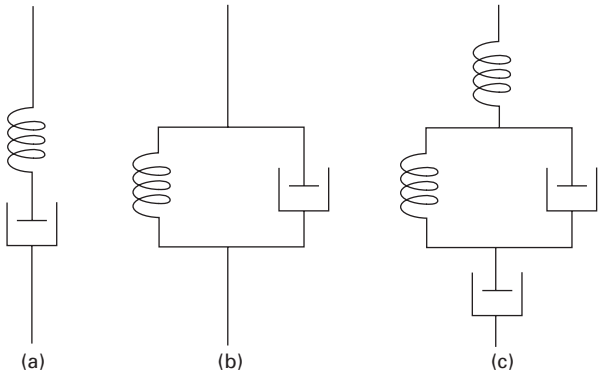

2.22 Spring-and-dashpot models of viscoelastic solids (a) Maxwell, (b) Voigt and (c) four-element model.

same and the total strain or strain rate is determined from the sum of the two components:

$$\frac{de}{dt} = \frac{\sigma}{\eta} + \frac{1}{E}\frac{d\sigma}{dt}$$

Voigt model

When the spring and dashpot are in parallel (Fig. 2.22(b)), the strains in the two elements are equal and the total stress on them is given by the sum:

$$\sigma_T(t) = Ee + \eta\frac{de}{dt}$$

If the applied stress is constant, as in a creep test, this differential equation may be directly integrated to give the strain as a function of time:

$$e(t) = \frac{\sigma}{E}(1 - e^{-t/\tau})$$

where the time constant, $\tau = \eta/E$.

Four-element model

A more realistic description of polymer behaviour is obtained with a four-element model consisting of Maxwell and Voigt elements in series (Fig. 2.22(c)). By combining the above equations, the total strain experienced by this model is given by:

$$e(t) = \frac{\sigma}{E_1} + \frac{\sigma}{E_2}(1 - e^{-t/\tau}) + \frac{\sigma}{\eta}t$$

© Woodhead Publishing Limited, 2006

It should be borne in mind that many additional elements are often required to represent adequately the mechanical behaviour of a given engineering polymer.

Having reviewed the *structure* of engineering materials and considered how their *mechanical properties* may be defined and measured, the remaining four chapters will explore the relationship between structure and properties, taking each family of materials in turn.

© Woodhead Publishing Limited, 2006